CrossMark

Increasing the availability of active sites in Zn-Co double metal cyanides by dispersion onto a SiO$_2$ support

Carlos Marquez [a], Miguel Rivera-Torrente [b], Pasi P. Paalanen [b], Bert M. Weckhuysen [b], Francisco G. Cirujano [a], Dirk De Vos [a,*], Trees De Baerdemaeker [a,c,*]

[a] Centre for Surface Chemistry and Catalysis, KU Leuven, Celestijnenlaan 200F, P.O. Box 2461, 3001 Leuven, Belgium
[b] Inorganic Chemistry and Catalysis, Debye Institute for Nanomaterials Science, Utrecht Universiteit, Universiteitsweg 99, 3584 CG Utrecht, The Netherlands
[c] Department of Chemistry, University of Oxford, Inorganic Chemistry Laboratory, South Parks Road, Oxford OX1 3QR, UK

ABSTRACT

Zn-Co double metal cyanides (DMCs) were dispersed on silica by dry and liquid-assisted (LAG) grinding to improve the catalytic performance of the DMC phase. The characterization of the resulting materials by transmission electron microscopy, N$_2$ physisorption, and powder X-ray diffraction indicated that the presence of water during the grinding step, not only helped to preserve the structural and textural properties of the DMC, but also facilitated the dispersion of the active phase onto the silica support. The accessibility of the Lewis acid sites was increased, as evidenced by FTIR spectroscopy with pyridine as probe molecule. The catalytic activity of the DMC phase for both the hydroamination of phenylacetylene with 4-isopropylaniline and the ring opening polymerization of 1,2-epoxyhexane was enhanced upon dispersion on silica due to the greater availability of the active Zn(II) sites. As a result, higher turnover frequencies were obtained upon decreasing the amount of DMC in the sample. The positive effect on the catalytic activity was the most pronounced for the catalysts prepared via LAG.

© 2017 The Authors. Published by Elsevier Inc. This is an open access article under the CC BY-NC-ND license (http://creativecommons.org/licenses/by-nc-nd/4.0/).

1. Introduction

Double metal cyanides (DMCs) are coordination polymers in which two different metals are connected through a cyanide group (C≡N). DMCs have the general formula $M^1_u[M^2(CN)_n]_v$, where the most common u-v combinations are 3–2, 1–1 and 4–3. For the 3–2 combination, M^1 is often a divalent metal, such as Zn(II), Fe(II), Co(II), or Ni(II); and $M^2(CN)_n$ is a hexacyanometallate anion of a trivalent metal such as Co(III), Fe(III) or Cr(III). The structure of these compounds is often cubic with a rock salt type ordering of $[M^1]^{v+}$ and $[M^2(CN)_6]^{u-}$, in which the $[M^2(CN)_6]^{u-}$ positions are only partially occupied to maintain charge neutrality [1–4]. Recently, DMCs have been investigated in diverse applications, for instance, in gas and energy storage [5–8]. In catalysis, they have been used since the 1960s, when the General Tire & Rubber company discovered their potential as catalyst for the ring opening polymerization of epoxides [9,10]. Since then, many studies have focused on new catalytic applications of DMCs in numerous reactions, notably, copolymerization of CO$_2$ and epoxides [11,12], esterification and transesterification [13–17], hydroamination [18,19], Prins condensation [20] and oxidation type reactions [21]. For epoxide ring-opening polymerization (ROP) reactions and hydroamination reactions, Zn$_3$[Co(CN)$_6$]$_2$ based materials (Zn-Co DMCs) show the best performance and the most promise in catalysis [18,22].

The synthesis of double metal cyanide compounds is relatively easy and normally involves a fast precipitation reaction after combining solutions of a water-soluble metal salt (M^1X_v) and a water-soluble metal cyanide salt ($Y_u[M^2(CN)_n]$) [23]. In order to increase the activity of the as-synthesized material, an excess of the metal salt (M^1X_v), and complexing (CAs) and co-complexing agents (co-CAs) are added to the synthesis mixture, especially in the case of Zn$_3$[Co(CN)$_6$]$_2$ based materials [22]. CAs are typically low molecular weight alcohols (e.g. ethanol, isopropanol, *n*-butanol, with tert-butanol being the most frequently used). Co–CAs are usually polyethers like poly(tetramethylene ether) glycol (PTMEG), polyethylene glycol (PEG) or Pluronic® P123 (P123) [19,24]. While the effect of these agents on the catalyst structure and activity is not entirely clear, co-CAs are believed to weakly coordinate to Zn(II) and Co(III) ions via hydroxyl groups during the nucleation process of the DMC, providing steric stabilization and preventing excessive particle growth [25].

In the cubic $Zn_3[Co(CN)_6]_2$, one third of the $[Co(CN)_6]^{3-}$ sites are vacant to maintain framework neutrality [3]. While these vacancies increase the micropore volume, the pores are usually too small ($\sim$5 Å) to allow diffusion of reactants and products, resulting in organic reactions mostly taking place on the external surface of the catalyst [19]. Several strategies have been suggested in order to increase the number of active sites available per mass of DMC. For example, Yi et al. [26] reported the synthesis of double and multi-metal cyanide nanoparticles (nano-sized DMCs) using a reverse emulsion technique, which increased the external surface area of the particles and further increased the catalytic activity of the materials for the copolymerization of CO_2 and cyclohexene oxide. More recently, the synthesis of hierarchically mesoporous M^1-M^2 DMCs (M^1 = Cu(II), Co(II) and Ni(II); and M^2 = Co(III)) in an ionic liquid/water/$MgCl_2$ system has been reported and the resulting materials were used for the electrochemical reduction of CO_2 to formic acid [27].

Another widely investigated strategy to improve the efficiency of catalytic processes is the immobilization of a catalytically active phase on a support, which can be useful to enhance the long-term performance of the catalyst while reducing the required amount of the catalytically active material [28–31]. For copolymerization reactions, SiO_2 and TiO_2 supported DMC catalysts prepared by co-precipitation of the DMC precursor salts and tetraethyl orthosilicate or titanium ethoxide were found to be active [32,33]. Here, we report the formation of supported Zn-Co DMC catalysts by simple grinding or ball milling in presence of a support. Our goal is to increase the accessibility of the active sites – i.e., the Zn(II) sites in the case of hydroamination and epoxide polymerization [19,22] – to achieve a higher turnover frequency (TOF). The effects of adding water during the grinding process (liquid assisted grinding, LAG), the support type and the DMC/support ratio are carefully investigated. The catalysts are characterized using transmission electron microscopy (TEM), Fourier transform infrared spectroscopy with pyridine as probe molecule (Py-FTIR), powder X-ray diffraction (PXRD) and N_2 physisorption and their catalytic performance was investigated in the hydroamination of phenylacetylene with 4-isopropylaniline and in the polymerization of 1,2-epoxyhexane.

2. Experimental section

2.1. Catalyst preparation

2.1.1. Preparation of reference DMCs

A reference DMC catalyst, referred to as DMC-PTMEG, was synthesized with CA (tert-butanol) and co-CA (PTMEG) according to literature procedures [18,34]. Solution A was prepared by dissolving 15 mmol of $ZnCl_2$ and 1.5 mmol of PTMEG (Sigma-Aldrich, average Mn $\sim$1000) in 150 ml of distilled water. Solution B was prepared by the addition of 1.5 mmol of $K_3[Co(CN)_6]$ to 15 ml of distilled water. Solution B was then added dropwise to solution A under vigorous stirring followed by the addition of 37.5 mL of tert-butanol (^tBuOH). The final mixture was stirred for 3 h at room temperature. The obtained solids were recovered by centrifugation and washed three times with a 50:50 mixture of water:^tBuOH. After drying at 333 K overnight, the solid product was ground to obtain a fine powder.

DMCs with high phase purity were synthesized following the procedures reported by Kuyper and Boxhoorn [35]. Both synthesis methods involve precipitation reactions between aqueous solutions of $ZnCl_2$ and $K_3[Co(CN)_6]$, without the presence of CA or co-CA. The rhombohedral phase is preferably obtained at higher temperature (373 K), from slightly more dilute solutions. The molar Zn/Co ratio in the synthesis of the rhombohedral modification cor-

responds to the stoichiometric ratio of 1.5, while for the cubic modification, a Zn/Co of 2.2 is used (Supporting information).

2.1.2. Preparation of silica-supported DMC catalysts by physical mixing (PM)

Specific amounts of DMC-PTMEG and 1 g of silica gel (Sigma-Aldrich, high purity grade, pore size 150 Å, 200–425 mesh) were ground for 15 minutes with an agate mortar and pestle set, with (LAG) and without water (0.6 ml). The solids were dried by heating under vacuum at 353 K overnight to obtain two series of silica-supported DMC catalysts: PM-X%$_{wet}$ and PM-X%$_{dry}$ where X refers to the wt.% of DMC in the solid. Additional supported DMCs were prepared under LAG conditions, using titanium oxide (AEROXIDE® TiO_2 P25) or zirconium (IV) oxide (Sigma-Aldrich, powder, 5 μm) as support.

2.1.3. Preparation of silica-supported DMC catalysts by ball milling (BM)

In order to understand the effect of the grinding process on the physicochemical properties of the material, a series of catalyst were prepared using ball milling. DMC-PTMEG was subjected to ball milling in a stainless steel grinding jar with two stainless steel grinding balls (7 mm diameter) without support for different times (2, 5, 10, 15 and 20 min) using a Retsch MM 400 ball mill at a frequency of 30 Hz. Additionally, specific amounts of DMC-PTMEG and 0.5 g silica gel, both with and without water (0.3 ml), were ball milled for 15 min under the same conditions to obtain two series of silica-supported DMC catalysts: BM-X%$_{wet}$ and BM-X%$_{dry}$ where X refers to the wt.% of DMC in the solid.

2.2. Catalyst characterization

The metal content of the catalysts was determined by ICP-OES analysis using a Varian 720-ES equipped with a double-pass glass cyclonic spray chamber, a Sea Spray concentric glass nebulizer and a high solids torch. The samples were digested using HF (aq). PXRD patterns were collected on a STOE Stadi MP diffractometer operating in transmission mode, using an image plate detector and focusing Ge(1 1 1) monochromator (Cu Kα_1 radiation, λ = 1.54060 Å), or on a Bruker D8 Advance eco diffractometer in Bragg-Brentano geometry with a LYNXEYE XE-T detector (CuKα_{12}), over a 10–60° 2θ range. N_2 physisorption isotherms were collected at 77 K on a Micromeritics 3Flex Surface Analyzer after evacuating the samples at 423 K for 16 h. The specific surface area (S_{BET}) was determined using the BET method (0.05–0.3 p/p$_0$), the specific external surface area (S_{ext}) and micropore volume (V_{micro}) were obtained using t-plot analysis and the median pore width was determined using the Horvath−Kawazoe model. TEM allowed the determination of DMC crystallite size and dispersion onto the support. Bright field measurements were obtained in a Tecnai T12 (FEI) microscope with a field emission gun operating at 120 kV. High angle annular dark field (HAADF) images and EDX maps were obtained in a Talos F200x (FEI), operated at 300 kV and equipped with high-brightness field emission gun (X-FEG) and a Super-X G2 EDX detector. Prior to imaging, the samples were gently ground, suspended in methanol and dropped onto a Cu grid (200 mesh) with holey carbon film. Pyridine adsorption followed by FTIR spectroscopy (Py-FTIR) was used to determine the acid site nature and density of the samples using a Nicolet 6700 FTIR spectrometer. A self-supporting wafer ($\sim$10 mg · cm^{-2}) was placed in a cell under vacuum and activated at 523 K for 1 h. The cell was cooled down and the probe molecule (25 mbar) was allowed to adsorb onto the wafer at 323 K until saturation. The physisorbed pyridine was removed by evacuation for 30 min before reheating to 423 K to record the IR spectrum. The acid site density was determined from the areas of the absorption bands corresponding to pyridine

coordinated to Lewis acid sites (1450 cm^{-1}) and using the integrated molar extinction coefficients of Emeis [36].

2.3. Catalytic reactions

2.3.1. Intermolecular hydroamination

Before reaction, the catalyst samples were activated at 353 K under vacuum overnight. Glass crimp cap reaction vials were loaded under N$_2$ atmosphere with 50 mg of catalyst, phenylacetylene (0.5 mmol), 4-isopropylaniline (1 mmol), dry toluene (1 ml) as solvent and tetradecane (1 mmol) as internal standard. The vials were placed in a heated copper block at 383 K and stirred at 500 rpm using a magnetic stirring bar. After reaction, the catalyst was removed by centrifugation and the liquid supernatant was analyzed by GC (Shimadzu 2014 GC equipped with a FID detector and a CP-Sil 5 CB column) and GC-MS (Agilent 6890 gas chromatograph, equipped with a HP-5MS column, coupled to a 5973 MSD mass spectrometer). Additional reactions with lower amounts of DMC-PTMEG were performed. After the reaction, the sample PM-9%$_{wet}$ was dried under vacuum and further characterized by XRD. Recycling test were performed after recovery and re-activation of the sample by drying at 353 K under vacuum overnight before each run.

2.3.2. Epoxide polymerization

Before reaction, the catalyst samples were activated at 353 K under vacuum overnight. Glass crimp cap reaction vials were loaded with 20 mg of catalyst, 1,2-epoxyhexane (2 mmol) and diethyleneglycol (0.2 mmol), under N$_2$ atmosphere. The reaction was carried out in a heated copper block at 383 K and stirred at 500 rpm using a magnetic stirring bar. After reaction, the product mixture was diluted in carbon disulfide (2.5 ml), and the catalyst was removed by centrifugation. The liquid supernatant was then collected in a 10.00 mm liquid cell for near-infrared measurements on a Cary 5000 UV-VIS-NIR spectrophotometer. The absorbance of the sample at 2220 nm was used to determine the epoxide conversion by correlation to the concentration of 1,2-epoxyhexane left in the reaction mixture using a calibration curve.

3. Results and discussion

3.1. Characterization

ICP analysis of DMC-PTMEG shows that the Zn/Co ratio is higher than the stoichiometric ratio of 1.5 expected for a phase pure cubic Zn$_3$[Co(CN)$_6$]$_2$ (Table S1, Supporting information). However, the PXRD pattern shows that DMC-PTMEG still consists predominantly of the cubic phase (e.g., peaks at 15°, 17.3° and 24.6° 2θ, Fig. 1) with

reflections at 14.5° and 23.6° 2θ indicating the presence of a small amount of the monoclinic phase [2,37]. This mixture of phases is consistent with previous reports of DMCs prepared using CAs and co-CAs [19].

PXRD patterns of ball milled DMC-PTMEG were collected after specific time points to follow structural changes and amorphization of the DMC during the grinding process without a support present (Fig. 1). As can be observed in Fig. 1a, without the presence of water during the ball milling process, changes in the structure of the material occur almost immediately (2 min), with amorphization taking place after only a few minutes of grinding. Moreover, a closer inspection of the patterns (Fig. S1, Supporting Information) shows the appearance of additional peaks at 16.4°, 19.8° and 21.8° 2θ, which are typical of a denser, more hydrophobic, rhombohedral phase of Zn$_3$[Co(CN)$_6$]$_2$ [38,39]. In contrast, under LAG conditions the crystalline structure of the solid remains more stable, with the pattern showing sharp reflections even after 20 min of grinding (Fig. 1b). No additional peaks are observed, indicating that no phase transformation occurs when water is present during the grinding process. The formation of the rhombohedral phase is possibly inhibited because under LAG conditions, there are always water molecules available that could readily coordinate to the zinc atoms, keeping the DMC in its cubic, hydrated form.

Comparable behavior is observed in the samples ball milled together with SiO$_2$ (Fig. 2). For both series, reflections assigned to the cubic DMC phase can be seen superimposed over the broad contribution of the amorphous silica. Once again, dry ball milling resulted in a notable destruction of the DMC structure and a partial phase transformation. In the case of the silica supported DMCs prepared by physical mixing (Fig. S2, Supporting Information), the effect of neat grinding is less pronounced, though for the sample PM-29%$_{wet}$, the reflections are still sharper than those observed in the PM-29%$_{dry}$ pattern. For the latter, the peaks assigned to the rhombohedral phase are also more intense.
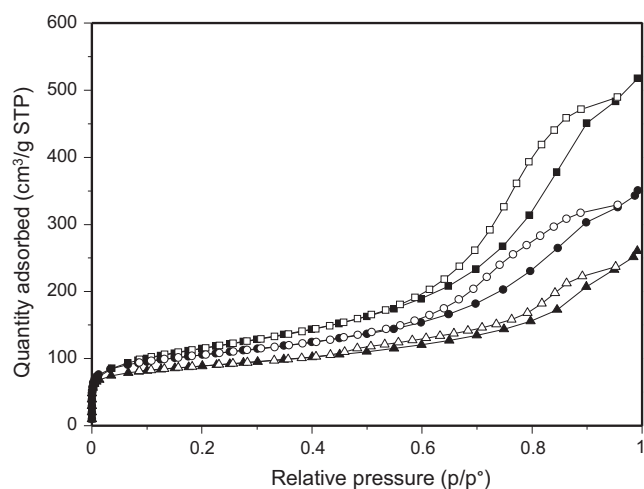
The N$_2$ physisorption isotherms obtained for the samples BM-9%$_{wet}$, BM-29%$_{wet}$ and BM-29%$_{dry}$ are shown in Fig. 3. All isotherms are a combination of the two starting materials: a type I isotherm, typical of microporous materials for DMC-PTMEG (median pore width = 0.6 nm) and a type IV isotherm for silica gel (Fig. S3, Supporting Information). A clear effect of the use of water during the grinding process is observed. In fact, liquid-assisted grinding resulted in a higher specific surface area and external surface area solid when compared to those prepared under dry ball milling conditions, as shown in Table 1. These results are in good agreement with the XRD characterization and suggest that with the presence of a solvent during the ball milling the crystalline structure of the material is preserved to a larger extent. Additionally, for a more diluted catalyst, BM-9%$_{wet}$, the values obtained for S_{BET} and S_{ext}
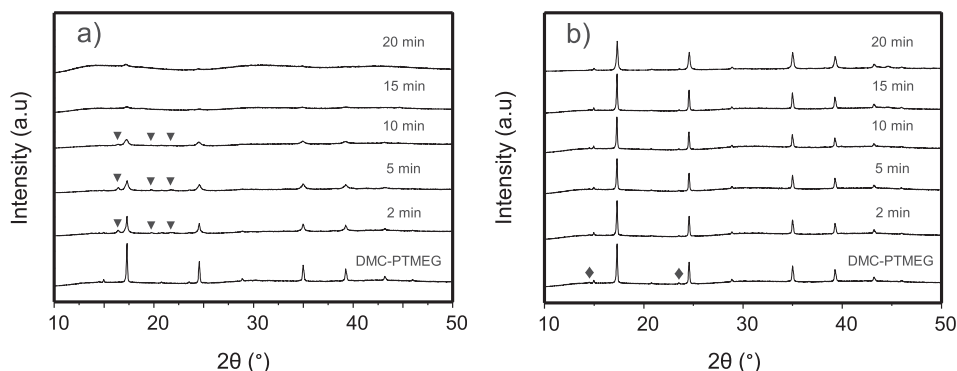
Fig. 1. XRD patterns of DMC-PTMEG after different grinding times: (a) dry grinding and (b) LAG. Reflections corresponding to the monoclinic phase are denoted by (♦) and to the rhombohedral phase by (▼).
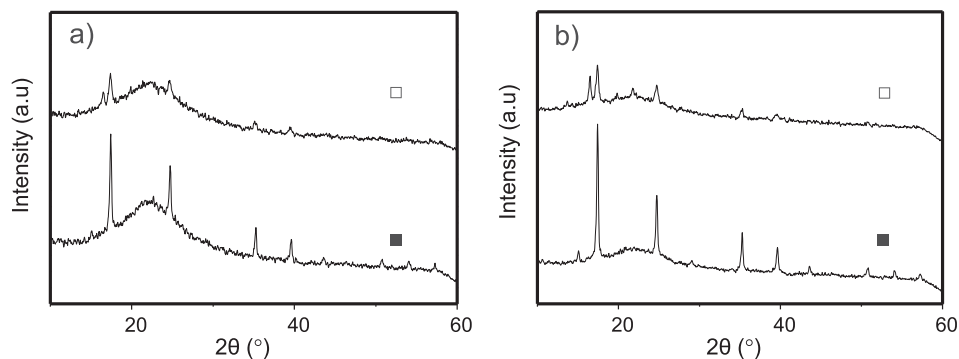
Fig. 2. XRD patterns of ball milled samples: (a) BM-9% prepared by (■) LAG and (□) dry grinding and (b) BM-29% prepared by (■) LAG and (□) dry grinding.

Fig. 3. Nitrogen physisorption isotherms of BM-9%$_{wet}$ (■/□), BM-29%$_{wet}$ (●/○) and BM-29%$_{dry}$ (▲/□). Filled symbols represents adsorption and open symbols, desorption.

Table 1
Textural properties determined from N$_2$ physisorption at 77 K of the starting materials and of selected samples.

Sample	S_{BET} (m²/g)	S_{ext} (m²/g)	V_{micro} (ml/g)
DMC-PTMEG	652	112	0.284
Silica gel	365	340	0.012
BM-9%$_{wet}$	400 (391)	332 (320)	0.033 (0.037)
BM-29%$_{wet}$	354 (448)	223 (274)	0.070 (0.091)
BM-29%$_{dry}$	292 (448)	155 (274)	0.066 (0.091)

Theoretically predicted weight averages from DMC-PTMEG and the support are showed in parenthesis.

are slightly higher than the weighted average of DMC-PTMEG and the support for these values, which in the case of S_{ext}, is indicative of the formation of smaller crystalline particles (Table 1). In contrast, for the samples containing a higher concentration of DMC – BM-29%$_{wet}$ and BM-29%$_{dry}$ – these values are lower than the weighted average, demonstrating the effect the ball milling process has on the textural properties of the supported catalysts.

TEM bright field images (Figs. 4 and S4, Supporting Information) show mostly supported, but also more isolated DMC crystals in close proximity to SiO$_2$. Even though size and morphology are barely modified during the ball milling process, the larger aggregates present in the DMC-PTMEG (>500 nm) were not detected after the ball milling process. For the samples prepared under LAG conditions, the DMC particles are in close contact with the support (Fig. 4a and b), whereas for the dry ball milled sample (Fig. 4c) a higher fraction of DMC crystals seems to be unsupported.

This suggest that the use of a solvent during the ball milling not only helps preserve the structural and textural properties of the DMC, but also facilitates the segregation of conglomerated DMC crystals and their dispersion onto the silica support. Furthermore, with parallel EDX elemental mapping (Fig. 4d and e), the close proximity between the support and the active phase for the sample BM-29%$_{wet}$ is clearly observed, with a considerable amount of DMC homogeneously supported and well dispersed onto the silica.

Pyridine adsorption followed by FTIR spectroscopy was used to probe the surface acidity of the synthesized materials. Fig. 5 shows the difference spectra obtained for the reference DMC and the silica-supported DMCs prepared by physical mixing under LAG conditions. The appearance of bands at 1610, 1492 and 1451 cm^{-1} indicates the presence of Lewis acid sites, whereas the absence of bands at 1639 and 1545 cm^{-1} denotes the lack of Brønsted acidity [40], showing that Zn-Co DMCs are purely Lewis acid catalysts. Furthermore, the low intensity of the 1575 cm^{-1} band means that the majority of the hydrogen-bonded pyridine is desorbed after heating at 423 K. The amount of pyridine adsorbed on Lewis acid sites per mass of DMC increases with the degree of dilution of DMC in the mixture (Table 2): from 0.11 mmol/g for DMC-PTMEG to 0.66 mmol/g for PM-9%$_{wet}$. This is a direct indication of the enhanced availability and accessibility of the Zn(II) Lewis acid sites upon dispersion of the DMC phase onto the support. The formation of Lewis-coordinated pyridine species is facilitated because of the greater exposure of surface Zn(II) sites, which is also suggested by the increase in S_{ext} observed with the decrease in the amount of DMC in the sample (Table 1).

3.2. Intermolecular hydroamination

#### 3.2.1. Silica supported DMCs

The catalytic activity of the silica-supported DMCs was first investigated for the intermolecular hydroamination of 4-isopropylaniline with phenylacetylene. The hydroamination results in the formation of an enamine that tautomerizes to a more stable imine (4-isopropylphenyl)(1-phenylethylidene)amine (Scheme 1) [18]. Hydroamination represents a green route towards the production of substituted amines [41,42]. Besides the fact that it is a 100% atom efficient reaction, the formation of side-products is limited: under these reaction conditions, only the formation of acetophenone as a side product was observed.

Fig. 6 shows the yield of the desired imine product for the unsupported DMC-PTMEG and the catalysts prepared by physical mixing under LAG conditions after 24 h reaction time. The corresponding space-time yield (STY) of the reaction can be found in Fig. S5, Supporting Information. As can be observed, with DMC-PTMEG (100 mg DMC per mmol of phenylacetylene) a high yield can be achieved (81%). Unsurprisingly, when the DMC loading is
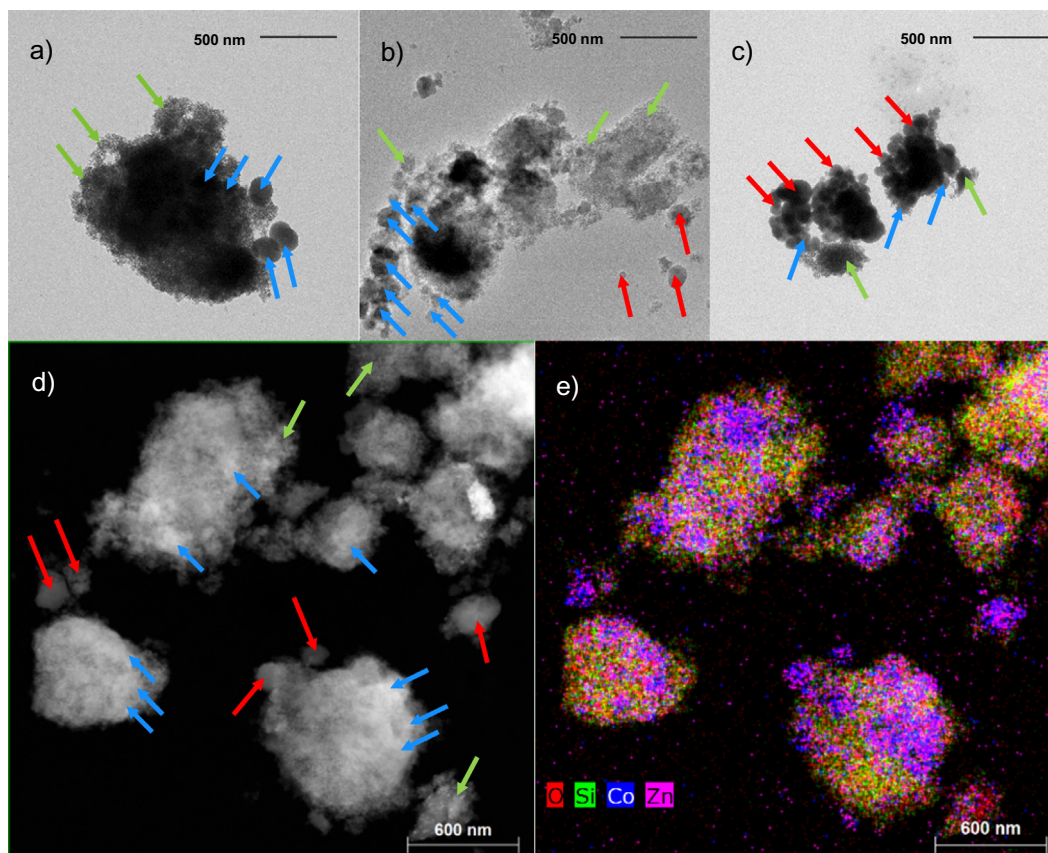
Fig. 4. TEM bright field images of samples BM-9%wet (a), BM-29%wet (b) and BM-29%dry (c); HAADF-STEM (d) and EDX composition map (e) of BM-29%wet. The green arrows indicate the SiO$_2$ support, the blue arrows the presence of DMC crystallites supported on SiO$_2$ and the red ones, unsupported DMC crystallites in close proximity to SiO$_2$.
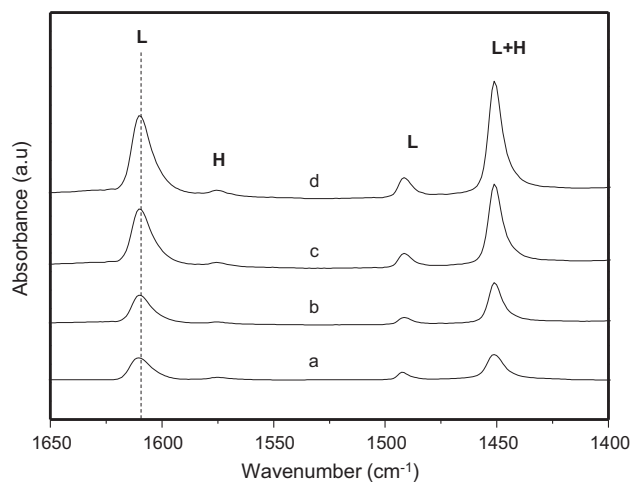
Fig. 5. Difference IR spectra of adsorbed pyridine (normalized to 10 mg of DMC/cm^2) for: (a) DMC-PTMEG, (b) PM 29%wet, (c) PM-17%wet and (d) PM 9%wet. Peaks corresponding to pyridine coordinated to Lewis acid sites (L) and hydrogen-bonded pyridine (H) are marked.

Table 2
Lewis acid properties as determined by FTIR analysis with pyridine as probe molecule.

Sample	LAS (mmol/g)[a]
DMC-PTMEG	0.11
PM-29%wet	0.14
PM-17%wet	0.28
PM-9%wet	0.66
Silica gel	n.d[b]

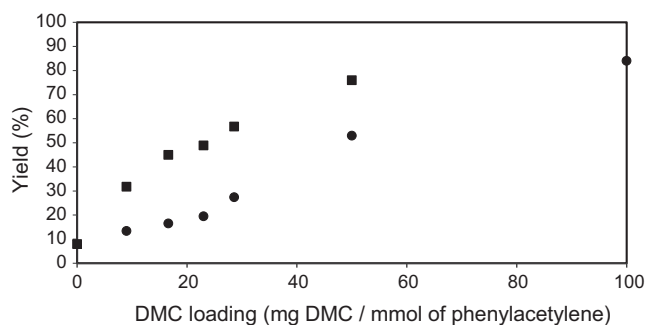[a] Amount of pyridine adsorbed on Lewis acid sites (LAS) per gram of DMC.
[b] Not detected.

ilar to the one obtained with the samples prepared by physical mixing. Furthermore, the DMC ground without the presence of silica, even under LAG conditions (PM-100%dry and PM-100%wet), showed the same activity as the original DMC-PTMEG (Table S2, Supporting Information).

To evaluate the activity of the DMC phase in the catalysts, the initial TOF of the Zn(II) sites (mol imine produced per mol Zn(II) per hour) was calculated. As can be observed in Fig. 7, the TOF increases with the degree of dilution of DMC in the sample, especially for the samples prepared under LAG conditions, which is in good agreement with the increased amount of pyridine adsorbed on Lewis acid sites as indicated by Py-FTIR spectroscopy. This further indicates that the availability of the Zn(II) sites is improved upon dispersion of the active phase onto the support. The Zn(II) sites – the active sites for this reaction [19] – are in this case more accessible to the reactant molecules causing the rise in catalytic activity.

reduced, the yield decreases; however, when the active phase is supported on silica, the imine production is largely maintained – even if the overall STY decreases compared to the unsupported DMC-PTMEG in the highest loading (100 mg DMC per mmol of phenylacetylene). For all investigated DMC:substrate ratios the imine production is substantially higher than the one achieved with the unsupported solid. For the ball milled samples (Table S2, Supporting Information), the yield obtained is very sim-

Scheme 1. Intermolecular hydroamination of 4-isopropylaniline with phenylacetylene.

Fig. 6. Yield of the hydroamination product after 24 h reaction time at 383 K for the silica supported DMCs prepared by physical mixing under LAG conditions (■), and for unsupported DMC-PTMEG (●).
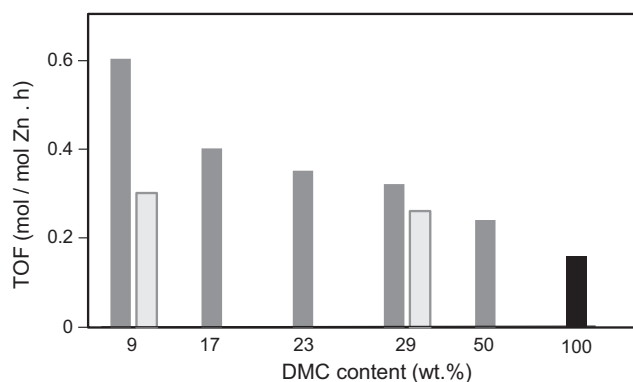
Fig. 7. Initial TOF (mol imine produced per mol Zn(II) per hour) for hydroamination of phenylacetylene at 383 K of DMC-PTMEG (■) and silica supported catalyst prepared by physical mixing under LAG (▦) and dry (▢) conditions.

The activity of the samples prepared by LAG is higher than the activity of samples prepared by dry grinding, especially at low DMC/support ratios (Fig. 7). XRD and N_2 sorption data showed that the presence of water helps to preserve the structural and the textural properties of the solid, in particular, the external surface area. Likewise, TEM images showed that a better dispersion of the DMC phase was obtained under LAG conditions, which would increase the accessibility of the Zn(II) sites. Moreover, the dry mixed catalysts also exhibited reflections attributed to the rhombohedral phase. In order to assess the relative activity of the phases, DMC catalysts with high phase purity (rhombohedral and cubic) were synthesized following the procedures reported by Kuyper and Boxhoorn [35]. The TOF for the cubic modification was found to be eleven times higher (Table S2, Supporting Information) than for the rhombohedral counterpart, which could be related to the lower density and hence, slightly higher accessibility of the cubic phase. This could partially contribute to the higher activity obtained for the liquid-assisted ground samples.

The pure-phased cubic material was also supported on silica (PM-9%$_{wet}$ – Cubic), and its activity was compared to the supported catalysts prepared with DMC-PTMEG (PM-9%$_{wet}$) (Table S2, Supporting Information). While the sample PM-9%$_{wet}$ – Cubic showed an increased activity relative to its unsupported counterpart, the activity was still inferior to the one exhibited by PM-9%$_{wet}$. The results are in agreement with previous reports that claim that the use of complexing and co-complexing agents, such as ^tBuOH and PTMEG, increase the activity of DMCs by affecting active site accessibility and particle size, while maintaining phase purity and crystallinity [19,25].

Recycling tests show that the catalyst largely maintains its activity after five runs (Fig. S6, Supporting Information), with no notable loss of crystallinity or change in the phase composition of the sample when compared to the pristine one (Fig. S7, Supporting Information). Furthermore, the heterogeneity of the catalyst was studied by a hot filtration test by removing the catalyst after 4 h of reaction time. Following this removal, no increase in conversion was observed after additional stirring for 20 h at 383 K (Fig. S8, Supporting Information). These results indicate that no catalytically active species leach from the catalyst.

3.2.2. Support scope

To appreciate the role of silica as support, the hydroamination reaction was repeated using ZrO_2 and TiO_2 as supports. These oxides were chosen because they are commonly used supports that normally exhibit catalytic properties on their own related to their Lewis acidity and their interaction with the active phase [33,43–45]. The supports showed poor catalytic activity without the presence of the DMC phase, producing the desired product only in low yields (Table S2, Supporting Information) even after 24 h of reaction. This again shows the important role the DMC plays as the active phase for the intermolecular hydroamination reaction.

Table 3 presents the initial TOFs (Zn(II) based) obtained for the DMC on different supports. The activity increases in the order $TiO_2 < ZrO_2 < SiO_2$; however, for all supports, a higher hydroamination activity is achieved for the more diluted sample, suggesting that the accessibility of the Zn(II) sites can be increased, regardless of the oxide.

A clearer difference in the activity of the supported samples is observed when the total imine product yield after 24 h reaction time is examined (Fig. 8). The yield of the desired imine product can be increased by 10% when SiO_2 is used as support instead of TiO_2 or ZrO_2. This could be an indication that the acidic properties of these oxides do not play an important role in the overall hydroamination activity of the catalyst and demonstrate that the silica gel, with its higher surface area, represents the best alternative of support. Further characterization of the catalysts and pure supports (Table S3, Supporting Information) shows that the

Table 3
Initial TOF for hydroamination of DMC supported on different oxides.

	Support		
	SiO$_2$	TiO$_2$	ZrO$_2$
PM-9%$_{wet}$	0.60	0.33	0.58
PM-29%$_{wet}$	0.34	0.17	0.27

TOF = mol imine produced per mol Zn(II) per h.
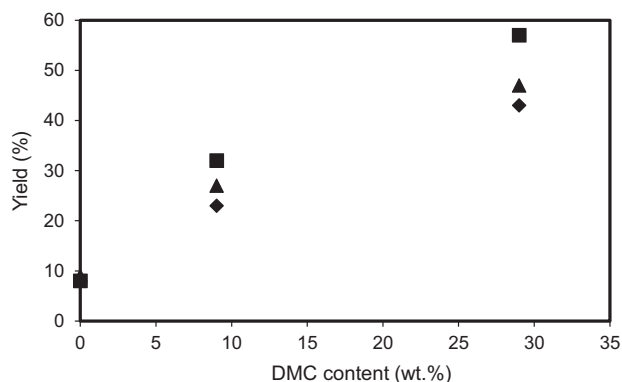
Fig. 8. Yield of the hydroamination product after 24 h reaction time at 383 K for the DMC samples supported on SiO₂ (■), ZrO₂ (▲) and TiO₂ (◆) prepared by physical mixing under LAG conditions.

dispersion of the acid sites, expressed as surface Lewis acid sites density, is increased when the DMC phase is supported on TiO₂ and SiO₂, while both the pure ZrO₂ and the ZrO₂-supported DMC present a higher concentration of Lewis acid sites on the external surface in comparison to the unsupported DMC-PTMEG. This low dispersion can be attributed to the low external surface area of the support.

These results are in contrast with previous studies [33], where the dispersion of DMC over TiO₂ had a better effect on the overall activity (superior chemoselectivity) relative to the DMC dispersion onto SiO₂ in the copolymerization of CO₂ with propylene oxide. However, in this case, the supports were formed simultaneously with the precipitation of the DMC phase via condensation of alkoxide precursors, likely resulting in different textural properties and surface species.
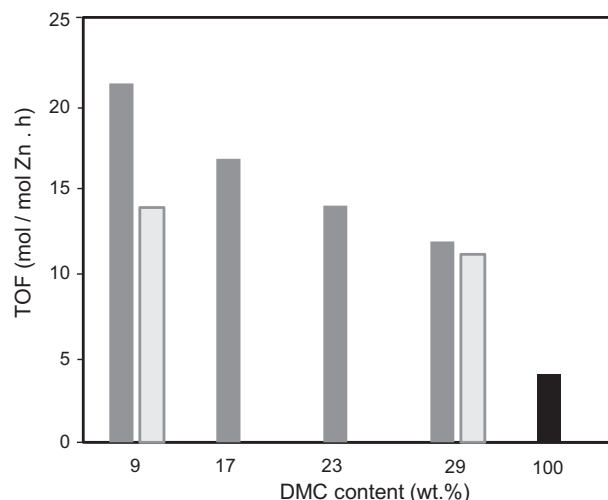
3.3. Epoxide polymerization

Ring opening polymerization of epoxides is one of the most important chemical processes catalyzed by double metal cyanides [46,47]. A reaction scheme of the polymerization of 1,2-epoxyhexane is presented in Scheme 2.

The initial TOF (mol epoxyhexane consumed per mol Zn(II) per hour) of the Zn(II) sites was calculated to gain information on the catalytic activity of the materials for this particular reaction. The dispersion of the DMC phase generated an increase in the catalytic activity, especially when the physical mixing process was carried out under LAG conditions (Fig. 9), reaching a TOF of 21.1 h^{-1} for PM-9%$_{wet}$.

For this reaction, the effect of the solvent during the dispersion process on the activity of the samples is once again very pronounced, especially at low DMC loadings, with the sample PM-9%$_{dry}$ showing a TOF of only 13.8 h^{-1}. This value is, however, still much higher than the one exhibited by the DMC-PTMEG (TOF of 4.1 h^{-1}), which is a clear indication that the availability and accessibility of the active sites can be increased by simple dispersion of the active phase onto a SiO₂. The activity shown by the samples prepared by ball milling is very similar to that exhibited by the samples prepared by physical mixing (Table S4, Supporting Information).
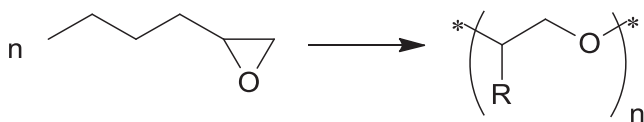
Fig. 9. Initial TOF (mol epoxyhexane consumed per mol Zn(II) per hour) for ring opening polymerization of 1,2-epoxyhexane at 383 K of DMC-PTMEG (■) and silica supported catalyst prepared by physical mixing under LAG (▨) and dry (▨) conditions.

4. Conclusions

The results presented here demonstrate that a highly active, stable and reusable supported DMC catalyst can be prepared by simple physical mixing methods. In the two reactions probed, the activity of the DMC phase was enhanced by supporting it onto silica, resulting in up to five times higher TOFs with a higher degree of dilution of the active phase. This catalytic result shows that the availability and accessibility of the Zn(II) sites are improved upon dispersion onto the support as was also indicated by TEM and FTIR characterization.

Both methods of preparation of the supported catalysts – physical mixing and ball milling – have a similar effect on the catalytic performance. In the hydroamination of phenylacetylene with 4-isopropylaniline, silica proved to be the best choice of support, although the accessibility of the active sites was increased regardless of the support used. These results could probably be related to its higher specific surface and external surface area, allowing a better dispersion of the active DMC phase.

The samples prepared under LAG conditions showed a higher activity when compared to the samples prepared under dry grinding conditions. The effect of water during the grinding process seems to be threefold: it helps to preserve the structural and textural properties of the DMC, promotes the dispersion of the DMC onto the support, and inhibits phase transformation from the cubic phase to the less active rhombohedral phase.

Overall, the results confirm that the number of active sites available in the DMC can easily be increased through physical mixing or ball milling with a suitable and simple support, such as silica. This implies that in order to achieve a high activity, lower amounts of the catalytically active material are required. These results will have direct implications for large scale applications, as further mechanical processing and shaping of the heterogeneous DMC catalyst with binders could seriously affect – and improve – the catalytic performance.

Scheme 2. Ring opening polymerization of 1,2-epoxyhexane. R: -(CH₂)₃CH₃.

Appendix A. Supplementary material

Detailed explanation of the synthesis of high phase purity DMCs, additional characterization data (ICP, XRD patterns, TEM images, N_2 physisorption isotherms) and tables containing catalytic data for the intermolecular hydroamination and the ring opening polymerization reactions can be found in the online version. Supplementary data associated with this article can be found, in the online version, at http://dx.doi.org/10.1016/j.jcat.2017.08.008.

References

[1] P. Valvekens, D. De Vos, in: New Materials for Catalytic Applications, Elsevier, Amsterdam, 2016, p. 1.
[2] D.F. Mullica, W.O. Milligan, G.W. Beall, W.L. Reeves, Crystal structure of $Zn_3[Co(CN)_6]_2 \cdot 12H_2O$, Acta Crystallogr., Sect. B 34 (1978) 3558–3561.
[3] A. Ludi, H.U. Guedel, M. Ruegg, The structural chemistry of Prussian blue analogs. A single-crystal study of manganese(II) hexacyanocobaltate(III), $Mn_3[CO(CN)_6]_2 \cdot xH_2O$, Inorg. Chem. 9 (1970) 2224–2227.
[4] G.W. Beall, W.O. Milligan, J. Korp, I. Bernal, Crystal structure of $Mn_3[CO(CN)_6]_2 \cdot 12H_2O$ and $Cd_3[Co(CN)_6]_2 \cdot 12H_2O$ by neutron and X-ray diffraction, Inorg. Chem. 16 (1977) 2715–2718.
[5] F.-M. Yang, Y. Liu, L. Chen, C.-T. Au, S.-F. Yina, Synthesis of amine-modified solid Fe-Zr adsorbents for CO_2 adsorption, J. Chem. Technol. Biotechnol. 91 (2016) 2340–2348.
[6] S.S. Kaye, J.R. Long, Hydrogen storage in the dehydrated Prussian blue analogues $M_3[Co(CN)_6]_2$ (M = Mn, Fe Co, Ni, Cu, Zn), J. Am. Chem. Soc. 127 (2005) 6506–6507.
[7] Y. Lu, L. Wang, J. Cheng, J.B. Goodenough, Prussian blue: a new framework of electrode materials for sodium batteries, Chem. Commun. 48 (2012) 6544–6546.
[8] C.D. Wessells, R.A. Huggins, Y. Cui, Copper hexacyanoferrate battery electrodes with long cycle life and high power, Nat. Commun. 2 (2011) 550.
[9] J. Milgrom, Method of making a polyether using a double metal cyanide complex, US Patent 3 278 457 (1966) to General Tire and Rubber Company.
[10] R.J. Herold, Method of making a polyether using a double metal cyanide complex. US Patent 3 278 457 (1966) to General Tire and Rubber Company.
[11] X.H. Zhang, S. Chen, X.M. Wu, X.K. Sun, F. Liu, G.R. Qi, Highly active double metal cyanide complexes: effect of central metal and ligand on reaction of epoxide/CO_2, Chin. Chem. Lett. 18 (2007) 887–890.
[12] J. Sebastian, D. Srinivas, Effects of method of preparation on catalytic activity of Co-Zn double-metal cyanide catalysts for copolymerization of CO_2 and epoxide, Appl. Catal. A 482 (2014) 300–308.
[13] R. Srivastava, D. Srinivas, P. Ratnasamy, Fe-Zn double-metal cyanide complexes as novel, solid transesterification catalysts, J. Catal. 241 (2006) 34–44.
[14] P.S. Sreeprasanth, R. Srivastava, D. Srinivas, P. Ratnasamy, Hydrophobic, solid acid catalysts for production of biofuels and lubricants, Appl. Catal. A 314 (2006) 148–159.
[15] J.K. Satyarthi, D. Srinivas, P. Ratnasamy, Influence of surface hydrophobicity on the esterification of fatty acids over solid catalysts, Energy Fuels 24 (2010) 2154–2161.
[16] J.K. Satyarthi, S. Radhakrishnan, D. Srinivas, Factors influencing the kinetics of esterification of fatty acids over solid acid catalysts, Energy Fuels 25 (2011) 4106–4112.
[17] M. Kotwal, S.S. Deshpande, D. Srinivas, Esterification of fatty acids with glycerol over Fe-Zn double-metal cyanide catalyst, Catal. Commun. 12 (2011) 1302–1306.
[18] A. Peeters, P. Valvekens, F. Vermoortele, R. Ameloot, C. Kirschhock, D. De Vos, Lewis acid double metal cyanide catalysts for hydroamination of phenylacetylene, Chem. Commun. 47 (2011) 4114–4116.
[19] A. Peeters, P. Valvekens, R. Ameloot, G. Sankar, C.E.A. Kirschhock, D. De Vos, Zn-Co double metal cyanides as heterogeneous catalysts for hydroamination: a structure-activity relationship, ACS Catal. 3 (2013) 597–607.
[20] M.V. Patil, M.K. Yadav, R.V. Jasra, Prins condensation for synthesis of nopol from β-pinene and paraformaldehyde on novel Fe–Zn double metal cyanide solid acid catalyst, J. Mol. Catal. A Chem. 273 (2007) 39–47.
[21] A. García-Ortiz, A. Grirrane, E. Reguera, H. García, Mixed (Fe^{2+} and Cu^{2+}) double metal hexacyanocobaltates as solid catalyst for the aerobic oxidation of oximes to carbonyl compounds, J. Catal. 311 (2014) 386–392.
[22] X.-H. Zhang, Z.-J. Huab, S. Chenc, F. Liua, X.-K. Suna, G.-R. Qi, Role of zinc chloride and complexing agents in highly active double metal cyanide catalysts for ring-opening polymerization of propylene oxide, Appl. Catal. A 325 (2007) 91–98.
[23] H. Liu, X. Wang, Y. Gu, W. Guo, Preparation and characterization of double metal cyanide complex catalysts, Molecules 8 (2003) 67–73.
[24] I. Kim, K.J. Lee, D.W. Park, B.U. Kim, C.S. Ha, Aliphatic polycarbonate synthesis by copolymerization of carbon dioxide with epoxides over double metal cyanide catalysts prepared by using ZnX_2 (X = F, Cl, Br, I), Catal. Today 111 (2006) 292–296.
[25] I.K. Lee, J.Y. Ha, C. Cao, D.-W. Park, C.-S. Ha, I. Kim, Effect of complexing agents of double metal cyanide catalyst on the copolymerizations of cyclohexene oxide and carbon dioxide, Catal. Today 148 (2009) 389–397.
[26] M.J. Yi, S.H. Byun, C.-S. Ha, D.-W. Park, I. Kim, Copolymerization of cyclohexene oxide with carbon dioxide over nano-sized multi-metal cyanide catalysts, Solid State Ionics 172 (2004) 139–144.
[27] X. Kang, X. Sun, Q. Zhu, X. Ma, H. Liu, J. Ma, Q. Qian, B. Han, Synthesis of hierarchical mesoporous Prussian blue analogues in ionic liquid/water/$MgCl_2$ and application in electrochemical reduction of CO_2, Green Chem. 18 (2016) 1869–1873.
[28] T. Blasco, A. Corma, A. Martínez, P. Martínez-Escolano, Supported heteropolyacid (HPW) catalysts for the continuous alkylation of isobutane with 2-butene: the benefit of using MCM-41 with larger pore diameters, J. Catal. 177 (1998) 306–313.
[29] T. De Baerdemaeker, M. Feyen, U. Müller, B. Yilmaz, F.-S. Xiao, W. Zhang, T. Yokoi, X. Bao, H. Gies, D.E. De Vos, Bimetallic Zn and Hf on silica catalysts for the conversion of ethanol to 1,3-butadiene, ACS Catal., 5 (2015) 3393–3397.
[30] I. Hermans, E. Breynaert, H. Poelman, R. De Gryse, D. Liang, G. Van Tendeloo, A. Maes, J. Peeters, P. Jacobs, Silica-supported chromium oxide: colloids as building blocks, Phys. Chem. Chem. Phys. 9 (2007) 5382–5386.
[31] G. Vilé, D. Baudouin, I.N. Remediakis, C. Copéret, N. López, J. Pérez-Ramírez, Silver nanoparticles for olefin production: new insights into the mechanistic description of propyne hydrogenation, ChemCatChem 5 (2013) 3750–3759.
[32] Y. Dienes, W. Leitner, M.G.J. Müller, W.K. Offermans, T. Reier, A. Reinholdt, T.E. Weirich, T.E. Müller, Hybrid sol-gel double metal cyanide catalysts for the copolymerisation of styrene oxide and CO_2, Green Chem. 14 (2012) 1168–1177.
[33] M.A. Subhani, C. Gürtler, W. Leitner, T.E. Müller, Nanoparticulate TiO_2-supported double metal cyanide catalyst for the copolymerization of CO_2 with propylene oxide, Eur. J. Inorg. Chem. 13–14 (2016) 1944–1949.
[34] I. Kim, J.T. Ahn, C.-S. Ha, C.S. Yang, I. Park, Polymerization of propylene oxide by using double metal cyanide catalysts and the application to polyurethane elastomer, Polymer 44 (2003) 3417–3428.
[35] J. Kuyper, G. Boxhoorn, Hexacyanometallate salts used as alkene-oxide polymerization catalysts and molecular sieves, J. Catal. 105 (1987) 163–174.
[36] C.A. Emeis, Determination of integrated molar extinction coefficients for infrared absorption bands of pyridine adsorbed on solid acid catalysts, J. Catal. 141 (1993) 347–354.
[37] J.C. Wojdel, S.T. Bromley, F. Illas, J.C. Jansen, Development of realistic models for Double Metal Cyanide catalyst active sites, J. Mol. Model. 13 (2007) 751–756.
[38] J. Roque, E. Reguera, J. Balmaseda, J. Rodríguez-Hernandez, L. Reguera, L.F. del Castillo, Porous hexacyanocobaltates(III): role of the metal on the framework properties, Micropor. Mesopor. Mater. 103 (2007) 57–71.
[39] C.P. Krap, B. Zamora, L. Reguera, E. Reguera, Stabilization of cubic and rhombohedral phases of zinc hexacyanocobaltate (III), Micropor. Mesopor. Mater. 120 (2009) 414–420.
[40] M. Orazov, M.E. Davis, Catalysis by framework zinc in silica-based molecular sieves, Chem. Sci. 7 (2016) 2264–2274.
[41] T.E. Müller, K.C. Hultzsch, M. Yus, F. Foubelo, M. Tada, Hydroamination: direct addition of amines to alkenes and alkynes, Chem. Rev. 108 (2008) 3795–3892.
[42] J. Penzien, T.E. Müller, J.A. Lercher, Hydroamination of 6-aminohex-1-yne over zinc based homogeneous and zeolite catalysts, Micropor. Mesopor. Mater. 48 (2001) 285–291.
[43] G.R. Bamwenda, S. Tsubota, T. Nakamura, M. Haruta, The influence of the preparation methods on the catalytic activity of platinum and gold supported on TiO_2 for CO oxidation, Catal. Lett. 44 (1997) 83–87.
[44] S.J. Tauster, S.C. Fung, R.T.K. Baker, J.A. Horsley, Strong interactions in supported-metal catalysts, Science 211 (1981) 1121–1125.
[45] P.D.L. Mercera, J.G. van Ommen, E.B.M. Doesburg, A.J. Burggraaf, J.R.H. Ross, Zirconia as a support for catalysts Influence of additives on the thermal stability of the porous texture of monoclinic zirconia, Appl. Catal. 71 (1991) 363–391.
[46] G. Trott, P.K. Saini, C.K. Williams, Catalysts for CO_2/epoxide ring-opening copolymerization, Phil. Trans. R. Soc. A 374 (2016) 20150085.
[47] S. Lee, S.T. Baek, K. Anas, C.-S. Ha, D.-W. Park, J.W. Lee, I. Kim, Tuning of activity, induction period and polymer properties of double metal cyanide catalyzed ring-opening polymerizations of propylene oxide by using quaternary ammonium salts, Polymer 48 (2007) 4361–4367.